Predictive-Adaptive Sliding Mode Control Method for Reluctance Actuator Maglev System

Yunlang Xu
Fudan University
Chenyang Ding
Fudan University
Xinyi Su
Fudan University
Zhi Li
Fudan University
Xiaofeng Yang (xf_yang@fudan.edu.cn)
Fudan University https://orcid.org/0000-0002-7027-3827

Research Article

Keywords: Nonlinearity, reluctance actuator, maglev system, sliding mode control, disturbance rejection

Posted Date: July 5th, 2022

DOI: https://doi.org/10.21203/rs.3.rs-1749421/v1

Predictive-Adaptive Sliding Mode Control Method for Reluctance Actuator Maglev System

Yunlang Xu · Chenyang Ding · Xinyi Su · Zhi Li · Xiaofeng Yang ✉

Received: date / Accepted: date

Abstract The control performance of reluctance actuator maglev system is seriously affected by inherent nonlinearities (e.g., hysteresis, eddy current, flux leakage, etc.) and external disturbances. To this end, this paper proposes an enhanced unknown system dynamics estimator (USDE)-based sliding mode control (USDE-SMC) method by a novel predictive-adaptive switching (PAS) controller (USDE-SMC-PAS). First, a USDE is incorporated into SMC to compensate for the uncertainties; Second, an adaptive switching (AS) controller is used to reduce chattering; Finally, the switching controller is modified by PAS to enhance the dynamic response ability and disturbance rejection ability with reduced chattering. In the PAS controller, the switching gain comprises a filtered estimate error part and a residual part, which are obtained by a first-order filter and an adaptive law, respectively. Consequently, the strong disturbance compensation ability, high levitation accuracy, high dynamic response, and reduced chattering property can be achieved simultaneously. The stabilities of USDE-SMC, USDE-SMC with an AS controller (USDE-SMC-AS), and USDE-SMC-PAS in the closed-loop system are analyzed by the Lyapunov theorem. Simulations and experiments are provided to validate the effectiveness and superior performance of the proposed method.

Keywords Nonlinearity · reluctance actuator · maglev system · sliding mode control · disturbance rejection

Yunlang Xu · Xiaofeng Yang ✉
State Key Laboratory of ASIC and System, School of Microelectronics, Fudan University, Shanghai, 200433, China.
E-mail: xuyunlang@fudan.edu.cn; xf_yang@fudan.edu.cn

Chenyang Ding · Xinyi Su
Shanghai Engineering Research Center of Ultra-Precision Motion Control and Measurement, Academy for Engineering and Technology, Fudan University, Shanghai, 200433, China.
E-mail: dingcy@fudan.edu.cn; xysu19@fudan.edu.cn

Zhi Li
State Key Laboratory of Synthetical Automation for Process Industries, Northeastern University, Shenyang 110819, China.
E-mail: lizhi1@mail.neu.edu.cn

1 Introduction

Reluctance actuators (i.e., electromagnetic actuators) have the advantages of large thrust and no contact, so they are widely used in magnetic levitation systems (MLSs)[1]. When the MLSs are used in semiconductor equipment, high levitation accuracy and high dynamic response are necessary for the control to satisfy the requirements of the production quality and production efficiency [2]. However, high performance control of reluctance actuators is challenging due to inherent nonlinearities [3] (e.g., hysteresis, eddy current, flux leakage, etc.) and external disturbances.

There are many advanced methods in the control of MLSs, including output feedback control [4],linear active disturbance rejection control (LADRC) method [5], adaptive backstepping control method [6], model predictive control (MPC) method [7], disturbance observer based control (DOBC) [8], adaptive fuzzy control method [9], and sliding mode control (SMC) [10] and so on. Among them, SMC is a method with simple structure but good control performance[11, 12, 13]. Recently, many SMC methods have been used for the control of MLSs, such as fractional-order SMC [14], PID-based SMC[15],high-order SMC[16], super-twisting SMC [17], and neural network adaptive SMC (NNASMC) [18], and so on. To enhance control performance, many researchers add additional disturbance compensation methods into SMC to deal with the uncertainties. Due to their strong generalization abilities, fuzzy logic systems (FLSs) [19] and neural networks (NNs) [20] have been embedded into SMC for uncertainty compensations, and they were successfully applied in MLSs. In NNs and FLSs, the weights need to be updated online, while this will imposes a heavy computational burden and cannot guarantee fast convergence of parameters [21]. On the other hand, the disturbance observer (DOB) methods, which can estimate and compensate for the uncertainties in the control synthesis, can also deal with the problem[22]. In [23], DOB is embedded into SMC to compensate for the nonlinear effects and model uncertainties in nanopositioning stages. Besides, nonlinear disturbance observer (NDOB) [24], adaptive disturbance observer(DOB) [25], extended disturbance observer (ESO) [26], generalized proportional integral observer (GPIO) [27], and unknown system dynamics estimator (USDE) [28] have also been developed for SMC to deal with unknown dynamics and disturbances. In the SMC methods with disturbance compensations, the residual compensation error must be suppressed by switching controller. However, due to the difficulty of obtaining accurate uncertainty bounds, excessive switching gain is unavoidable to ensure robustness, which may introduce obvious chattering and finally cause mechanical and electronic damage to MLS.

Recently, adaptive SMC methods, which can update the switching gain in a dynamic adaption way, are popular for balancing the chattering and the robustness. In [29], a threshold-based adaptive law which is updated by the distance of the system state to a discontinuity surface was proposed. In [30], an adaptive SMC strategy without under-estimation and over-estimation was proposed, which stops increasing (resp. decreasing) the control gain when the tracking error decreases (resp. increases). In [31], the switching gain of SMC was updated by an integral/exponential adaptation law for chattering reduction. In [32], the upper bound of uncertainty was designed by a NN, and the switching gain of SMC was updated by the adaptive NN. In [33], a new adaption law with arbitrarily small vicinity of the sliding manifold was presented for the chattering reduction, which is inversely proportional to the sliding variables. In [34], the uncertainty upper bound was designed as a first-order polynomial, and thus the switching gain is adaptively updated by the polynomial with adaptive coefficients. However, although the existing adaptive SMC methods can ensure that the switching gain converges to the vicinity of the actual boundary value finally, there will be a significant difference between the switching gain and the actual boundary value during the dynamic process. The dynamic response performance thus will be sacrificed.

Considering that the switching controller is mainly used to deal with the compensation error, if the estimate error of USDE can be embedded in the switching gain, it may be possible to improve the dynamic response performance. To this end, this paper proposes an enhanced USDE-based SMC (USDE-SMC) method by a predictive-adaptive switching (PAS) controller (USDE-SMC-PAS). The switching gain of the PAS controller is composed of a filtered estimate error part and an adaptive residual part to obtain higher dynamic response and stronger robustness. The main contributions lie in:

1. A USDE-SMC-PAS method is designed for reluctance actuator maglev system for robustness enhancement and chattering reducing synchronously, where the PAS controller is updated by a filtered estimate error and an adaption law.
2. A filtered estimate error of USDE is directly deduced, and an estimate error-based dynamic upper bound about the uncertainty is designed.
3. A USDE-SMC-AS is also constructed for the maglev system by embedding an adaptive switching (AS) controller into the traditional USDE-SMC.
4. The stabilities about USDE-SMC, USDE-SMC-AS, and USDE-SMC-PAS in the closed-loop system are analyzed.

The rest of this paper is organized as follows: In Section II, the mathematical model of an MLS is introduced; The new control scheme is proposed in Section III; The simulations are performed in Section IV; The experiments are conduced in Section V; Finally, Section VI concludes the paper.

2 Modeling of maglev system

The structure of the maglev plant is shown in Fig.1. It is composed of a levitation reluctance actuator and a disturbance injection reluctance actuator. The levitation reluctance actuator contains a bottom E-mover and an I-target, and the disturbance injection reluctance actuator contains a top E-mover and an I-target. The E-movers and the I-target are laminated by silicon-iron materials. The excitation currents are i and i_d for the levitation and disturbance injection actuators, respectively. The parameters are set as Table 1.

Assume that the magnetic field in the reluctance actuator is uniformly distributed, it can be obtained according to the Maxwell equation

$$Ni = l_{Fe}H + \frac{2x}{\mu_0}B \tag{1}$$

where l_{Fe} is the length of the flux linkage, H is the magnetic field intensity, μ_0 denotes the air permeability

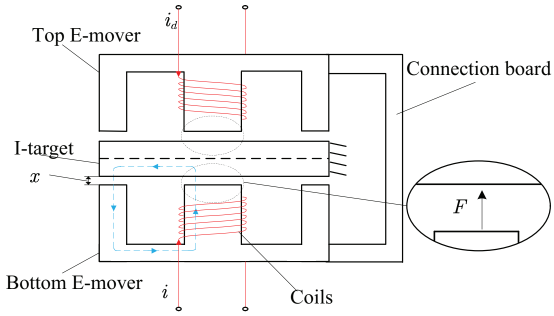

Fig. 1: Electromagnetic actuators with an EI-type structure.

Table 1: Parameter values of the MLS

Physical quantity	Value
Coil turns N	280
Air permeability μ_0	4×10^{-7} N/A^2
Mass m	3.233 kg
Gravitational acceleration g	9.8 m/s^2
Cross sectional area A	2.88×10^{-4} m^2

and x denotes the levitation position. If the effects of hysteresis, eddy current and flux leakage are omitted, we have $H = \frac{B}{\mu_0\mu_r}$. Therefore,

$$B = \frac{\mu_0 N i}{\frac{l_{Fe}}{\mu_r} + 2x} + B_n(x) \tag{2}$$

where μ_r is relative permeability in silicon-iron and $B_n(x)$ represents the flux caused by the nonlinearities including hysteresis, eddy current and flux leakage. $\frac{l_{Fe}}{\mu_r} \ll 2x$, and thus it can be omitted. According to Maxwell's stress tensor, the relationship between the output force F and the flux density B can be calculated as

$$F = \frac{B^2 A}{2\mu_0} = \frac{\mu_0 A N^2 i^2}{8x^2} + \frac{B_n^2(x) A}{2\mu_0}. \tag{3}$$

Denoting $K(x) = \frac{\mu_0 A N^2}{8x^2}$, the actual dynamic model of MLS can be given as

$$(m+\delta_m)\ddot{x} = (m+\delta_m) g - K(x) i^2 - \frac{B_n^2(x) A}{2\mu_0} + F_d. \tag{4}$$

where δ_m is the deviations of the parameters m, and F_d represents the external disturbances. A lumped uncertainty can be defined as

$$L_d = -\frac{1}{m}\left(-\delta_m g + \delta_m \ddot{x} + \frac{B_n^2(x) A}{2\mu_0} - F_d\right) \tag{5}$$

Linearizing the MLS by using $i = \sqrt{\frac{mu}{K(x)}}$ $(u > 0)$, the dynamic of the MLS can be deduced as

$$\begin{cases} \dot{x}_1 = x_2 \\ \dot{x}_2 = -u + g - L_d \\ y = x_1. \end{cases} \tag{6}$$

where $[x_1 \;\; x_2]^{\mathrm{T}} = [x \;\; \dot{x}]^{\mathrm{T}}$.

Assumption 1 *[35] Assume L_d is bounded. It satisfies $|L_d| < L_d^u$ where L_d^u is a positive constant, and the derivative of L_d is bounded by $\sup_{t\geq 0}\left|\dot{L}_d\right| \leq \vartheta$ where ϑ is a positive constant.*

3 Controller design

In an MLS control system, the tracking error and its derivative with respect to time are given by

$$\begin{cases} e = r - x_1 \\ \dot{e} = \dot{r} - \dot{x}_1 = \dot{r} - x_2 \end{cases} \tag{7}$$

where r is a given trajectory. Based on the tracking error e and the derivative $\dot{e}$, a sliding mode variable S and its derivative with respect to time $\dot{S}$ are designed as

$$\begin{cases} S = \dot{e} + \lambda e \\ \dot{S} = \ddot{r} - \dot{x}_2 + \lambda\dot{e} = u + \ddot{r} - g + L_d + \lambda\dot{e} \end{cases} \tag{8}$$

where λ is a positive control gain.

3.1 The design of USDE-SMC

To compensate for the lumped uncertainty L_d, a USDE is used. Herein, the filter variables x_{2f} and u_f are defined as

$$\begin{cases} \kappa\dot{x}_{2f} + x_{2f} = x_2, x_{2f}(0) = 0 \\ \kappa\dot{u}_f + u_f = u, u_f(0) = 0 \end{cases} \tag{9}$$

where κ is a positive constant which determines the bandwidth of the low-pass filters. The following Lemma can be obtained.

Lemma 1 *[35] Considering system (6) and the filter variables in (9), an invariant manifold for any positive constant κ can be defined as*

$$\gamma = \frac{x_2 - x_{2f}}{\kappa} + u_f - g + L_d. \tag{10}$$

γ satisfies $\lim_{\kappa\to 0}\left[\lim_{t\to\infty}\gamma\right] = 0$.

Therefore, L_d can be estimated as

$$\hat{L}_d = -u_f + g - \frac{x_2 - x_{2f}}{\kappa}. \tag{11}$$

Adding a filter $\frac{1}{1+\kappa s}$ (s represents the laplace variable) into (6), one obtains

$$\frac{1}{1+\kappa s}[\dot{x}_2] = -\frac{1}{1+\kappa s}[u] + \frac{1}{1+\kappa s}[g - L_d]. \tag{12}$$

Defining $L_{df} = \frac{1}{1+\kappa s}[L_d]$ and considering $\dot{x}_{2f} = \frac{x_2 - x_{2f}}{\kappa}$, one obtains

$$L_{df} = -u_f + g - \frac{x_2 - x_{2f}}{\kappa}. \tag{13}$$

Comparing both (11) and (13), it can be deduced that $L_{df} = \hat{L}_d$. Therefore, the estimate error e_L can be deduced as

$$e_L = L_d - \hat{L}_d = \frac{\kappa s}{1+\kappa s}[L_d]. \tag{14}$$

Furthermore, one obtains [36]

$$\dot{e}_L = -\frac{1}{\kappa}e_L + \dot{L}_d. \tag{15}$$

The estimation error e_L is bounded by[36]

$$|e_L| \leq \sqrt{e_L^2(0)e^{-t/\kappa} + \kappa^2\vartheta^2}. \tag{16}$$

The control law of the USDE-SMC is designed as

$$u = -\lambda\dot{e} - \ddot{r} + g - \Lambda S - \hat{L}_d - \rho\,\mathrm{sgn}(S) \tag{17}$$

where Λ is a positive gain and ρ is the switching gain. $-\hat{L}_d$ and $-\rho\,\mathrm{sgn}(S)$ represent the USDE compensator and the switching controller, respectively.

Theorem 1 *The closed-loop trajectories in (6) with the control law (17) are globally uniformly ultimately bounded (GUUB), if $\rho \geq |e_L|$.*

Proof A Lyapunov function is chosen as

$$V_1 = \frac{1}{2}S^2 + \frac{1}{2}e_L^2. \tag{18}$$

The derivative of V_1 with respect to time is expressed as

$$\begin{aligned}\dot{V}_1 &= S\dot{S} + e_L\dot{e}_L \\ &= S(u + \ddot{r} - g + L_d + \lambda\dot{e}) + e_L\left(-\frac{1}{\kappa}e_L + \dot{L}_d\right) \\ &= -\Lambda S^2 - \frac{1}{\kappa}e_L^2 - (\rho|S| - e_L S) + e_L\dot{L}_d\end{aligned} \tag{19}$$

where $e_L\dot{L}_d \leq \frac{1}{2\kappa}e_L^2 + \frac{\kappa}{2}\dot{L}_d^2 \leq \frac{1}{2\kappa}e_L^2 + \frac{\kappa}{2}\vartheta^2$ and $\rho - |e_L| > 0$. Thus,

$$\dot{V}_1 \leq -\beta_1 V_2 + \frac{1}{2}\kappa\vartheta^2 \tag{20}$$

where $\beta_1 = \min\left\{2\Lambda, \frac{1}{\kappa}\right\}$. Using $0 < \beta_2 < \beta_1$, (20) can be further simplified as

$$\dot{V}_1 \leq -\beta_2 V_1 - (\beta_1 - \beta_2)V_1 + \frac{1}{2}\kappa\vartheta^2 \tag{21}$$

When $V_1 \geq \frac{\kappa\vartheta^2}{2(\beta_1 - \beta_2)}$, $\dot{V}_1 \leq 0$. Thus,

$$V_1 \leq \max\left\{V_1(0), \frac{\kappa\vartheta^2}{2(\beta_1 - \beta_2)}\right\}, \forall t \geq 0. \tag{22}$$

According to (18), it can be seen that $\frac{1}{2}S^2 \leq V_1$. Therefore, $|S| \leq \sqrt{\frac{\kappa\vartheta^2}{(\beta_1 - \beta_2)}}$. It is concluded that closed-loop system is GUUB.

3.2 The design of USDE-SMC-AS

Defining K as the upper bound about the compensation error e_L, where $K \geq |e_L|$. The control law of the USDE-SMC-AS is designed as

$$\begin{cases} u = -\lambda\dot{e} - \ddot{r} + g - \Lambda S - \hat{L}_d + u_{as} \\ u_{as} = -\hat{K}\mathrm{sgn}(S) \end{cases} \tag{23}$$

where u_{as} represents the adaptive switching controller. $\hat{K}$ is the estimate of K, updated by

$$\dot{\hat{K}} = \Gamma\left(|S| - \Upsilon\hat{K}\right) \tag{24}$$

where Γ and Υ are positive constants, and $\hat{K}(0) > 0$. It can be concluded that $\hat{K} \geq 0$, due to

$$\begin{aligned}\hat{K}(t) &= \exp(-\Upsilon t)\hat{K}(0) \\ &\quad + \int_0^t \exp(-\Upsilon(t-\tau))(|S||e_{Lf}|)\,d\tau \geq 0.\end{aligned} \tag{25}$$

Theorem 2 *The closed-loop trajectories in (6) with the control law (23), the adaptive law (24), and the estimator (11) are GUUB.*

Proof A Lyapunov function is chosen as

$$V_2 = \frac{1}{2}S^2 + \frac{1}{2}e_L^2 + \frac{1}{2\Gamma}\tilde{K} \tag{26}$$

where $\tilde{K} = \hat{K} - K$. The derivative of V_2 with respect to time is expressed as

$$\begin{aligned}\dot{V}_2 &= S\dot{S} + e_L\dot{e}_L + \Gamma\tilde{K}\dot{\hat{K}} \\ &= S(u + \ddot{r} - g + L_d + \lambda\dot{e}) + e_L\left(-\frac{1}{\kappa}e_L + \dot{L}_d\right) \\ &\quad + \frac{1}{\Gamma}\tilde{K}\dot{\hat{K}} \\ &\leq -\Lambda S^2 - \frac{1}{\kappa}e_L^2 - \left(\hat{K} - |e_L|\right)|S| + e_L\dot{L}_d \\ &\quad + \frac{1}{\Gamma}\tilde{K}\dot{\hat{K}}\end{aligned} \tag{27}$$

where $-\left(\hat{K} - e_L\right) \leq K - \hat{K} = -\tilde{K}$ and $e_L\dot{L}_d \leq \frac{1}{2\kappa}e_L^2 + \frac{\kappa}{2}\dot{L}_d^2 \leq \frac{1}{2\kappa}e_L^2 + \frac{\kappa}{2}\vartheta^2$. Therefore,

$$\dot{V}_2 \leq -\Lambda S^2 - \frac{1}{2\kappa}e_L^2 + \frac{1}{2}\kappa\vartheta^2 + \tilde{K}\left(\frac{1}{\Gamma}\dot{\hat{K}} - |S|\right). \tag{28}$$

Substituting (24) into (28), one obtains

$$\dot{V}_2 \le -\Lambda S^2 - \frac{1}{2\kappa} e_L^2 + \frac{1}{2}\kappa\vartheta^2 + \Upsilon \hat{K} K - \Upsilon \hat{K}^2 \tag{29}$$

where $\hat{K}K - \hat{K}^2 = -\frac{1}{2}\left(\hat{K} - K\right)^2 + \frac{1}{2}K^2 - \frac{1}{2}\hat{K}^2 \le -\frac{1}{2}\tilde{K}^2 + \frac{1}{2}K^2$. Thus,

$$\dot{V}_2 \le -\Lambda S^2 - \frac{1}{2\kappa} e_L^2 - \frac{\Upsilon}{2}\tilde{K}^2 + \frac{1}{2}\kappa\vartheta^2 + \frac{\Upsilon}{2}K^2. \tag{30}$$

Defining $\beta_3 = \min\left\{2\Lambda, \frac{1}{\kappa}, \Upsilon\right\}$, $\dot{V}_2$ can be further concluded as

$$\dot{V}_2 \le -\beta_3 V_2 + \frac{1}{2}\kappa\vartheta^2 + \frac{\Upsilon}{2}K^2 \tag{31}$$

Using $0 < \beta_4 < \beta_3$, (31) can be further simplified as

$$\dot{V}_2 \le -\beta_4 V_2 - (\beta_3 - \beta_4) V_2 + \Xi \tag{32}$$

where $\Xi = \frac{1}{2}\kappa\vartheta^2 + \frac{\Upsilon}{2}K^2 > 0$. When $V_2 \ge \frac{\Xi}{\beta_3 - \beta_4}$, $\dot{V}_2 \le 0$. Thus,

$$V_2 \le \max\left\{V_2(0), \frac{\Xi}{\beta_3 - \beta_4}\right\}, \forall t \ge 0. \tag{33}$$

According to (26), it can be seen that $\frac{1}{2}S^2 \le V_2$. Therefore, $|S| \le \sqrt{\frac{2\Xi}{\beta_3 - \beta_4}}$. It is concluded that closed-loop system is GUUB.

3.3 The design of USDE-SMC-PAS

Considering that the switching controller after USDE compensation is mainly used to deal with the compensation error, USDE-SMC-PAS (as shown in Fig. 2) designs a filtered estimate error-based dynamic upper bound about the uncertainty, to improve the dynamic response performance.

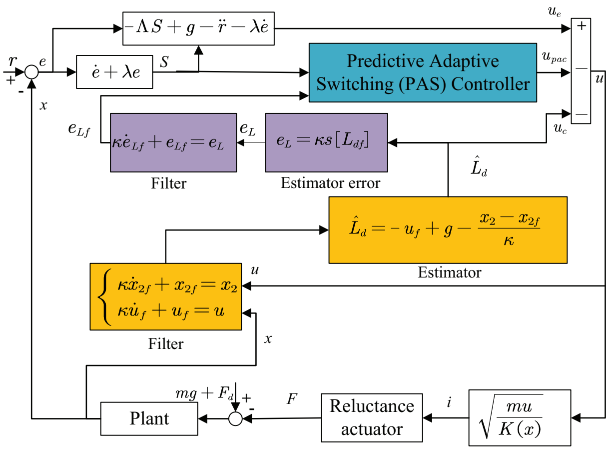

Fig. 2: The structure of USDE-SMC-PAS.

Defining e_{Lf} as the filtered variable about e_L, it can be deduced that

$$\kappa\dot{e}_{Lf} + e_{Lf} = e_L, e_{Lf}(0) = 0. \tag{34}$$

Considering both (14) and (34), one obtains

$$\kappa\dot{e}_{Lf} + e_{Lf} = \frac{\kappa s}{1 + \kappa s}[L_d]. \tag{35}$$

Therefore,

$$e_{Lf} = \frac{\kappa s}{1 + \kappa s}[L_{df}]. \tag{36}$$

A filtered estimate error-based dynamic upper bound about the compensation error e_L can be defined as

$$e_L \le |e_{Lf}| + \epsilon \tag{37}$$

where $|e_{Lf}|$ and ϵ ($\epsilon > 0$) represent the filtered estimate error part and the residual part, respectively. Based on the dynamic bound, the control law of the USDE-SMC-PAS is designed as

$$\begin{cases} u = u_e + u_c + u_{pas} \\ u_e = -\lambda\dot{e} - \ddot{r} + g - \Lambda S \\ u_c = -\hat{L}_d \\ u_{pas} = -\left(|e_{Lf}| + \hat{\epsilon}\right)\operatorname{sgn}(S) \end{cases} \tag{38}$$

where u_e, u_c, and u_{pas} represent the equivalent controller, the USDE compensator, and the PAS controller. $\hat{\epsilon}$ is the estimate of ϵ, updated by

$$\dot{\hat{\epsilon}} = \Gamma_\epsilon\left(|S| - \Upsilon_\epsilon\hat{\epsilon}\right) \tag{39}$$

where Γ_ϵ and Υ_ϵ are positive constants, and $\hat{\epsilon}(0) > 0$. It can concluded that $\hat{\epsilon} \ge 0$, due to

$$\hat{\epsilon}(t) = \exp\left(-\Upsilon_\epsilon t\right)\hat{\epsilon}(0) + \int_0^t \exp\left(-\Upsilon_\epsilon(t - \tau)\right)\left(|S|\,|e_{Lf}|\right)d\tau \ge 0. \tag{40}$$

Theorem 3 *The closed-loop trajectories in (6) with the control law (38), the adaptive law (39), the estimator (11), and the filter (36) are GUUB.*

Proof A Lyapunov function is chosen as

$$V_3 = \frac{1}{2}S^2 + \frac{1}{2}e_L^2 + \frac{1}{2\Gamma_\epsilon}\tilde{\epsilon}^2 \tag{41}$$

where $\tilde{\epsilon} = \hat{\epsilon} - \epsilon$. The derivative of V_3 with respect to time is expressed as

$$\begin{aligned} \dot{V}_3 &= S\dot{S} + e_L\dot{e}_L + \frac{1}{\Gamma_\epsilon}\tilde{\epsilon}\dot{\hat{\epsilon}} \\ &= S\left(-\Lambda S + e_L - \left(|e_{Lf}| + \hat{\epsilon}\right)\operatorname{sgn}(S)\right) \\ &\quad + e_L\left(-\frac{1}{\kappa}e_L + \dot{L}_d\right) + \frac{1}{\Gamma_\epsilon}\tilde{\epsilon}\dot{\hat{\epsilon}}. \end{aligned} \tag{42}$$

Considering (37), one obtains $e_L - (|e_{Lf}| + \hat{\epsilon}) \le |e_{Lf}| + \epsilon - (|e_{Lf}| + \hat{\epsilon}) \le -\tilde{\epsilon}$. Using $e_L \dot{L}_d \le \frac{1}{2\kappa} e_L^2 + \frac{\kappa}{2} \dot{L}_d^2 \le \frac{1}{2\kappa} e_L^2 + \frac{\kappa}{2} \vartheta^2$ and (39) , one obtains

$$\dot{V}_3 \le -\Lambda S^2 - \frac{1}{2\kappa} e_L^2 + \frac{1}{2}\kappa \vartheta^2 + \Upsilon_\epsilon \hat{\epsilon}\epsilon - \Upsilon_\epsilon \hat{\epsilon}^2 \tag{43}$$

where $\hat{\epsilon}\epsilon - \hat{\epsilon}^2 \le -\frac{1}{2}\tilde{\epsilon}^2 + \frac{1}{2}\epsilon^2$. Therefore,

$$\dot{V}_3 \le -\Lambda S^2 - \frac{1}{2\kappa} e_L^2 - \frac{\Upsilon_\epsilon}{2}\tilde{\epsilon}^2 + \frac{1}{2}\kappa \vartheta^2 + \frac{\Upsilon_\epsilon}{2}\epsilon^2. \tag{44}$$

Defining $\beta_5 = \min\left\{2\Lambda, \frac{1}{\kappa}, \Upsilon_\epsilon\right\}$, $\dot{V}_3$ can be concluded as

$$\dot{V}_3 \le -\beta_5 V_3 + \frac{1}{2}\kappa \vartheta^2 + \frac{\Upsilon_\epsilon}{2}\epsilon^2. \tag{45}$$

Using $0 < \beta_6 < \beta_5$, (45) can be further simplified as

$$\dot{V}_3 \le -\beta_6 V_3 - (\beta_5 - \beta_6) V_3 + \Xi_\epsilon \tag{46}$$

where $\Xi_\epsilon = \frac{1}{2}\kappa\vartheta^2 + \frac{\Upsilon_\epsilon}{2}\epsilon^2 > 0$. When $V_3 \ge \frac{\Xi_\epsilon}{\beta_5 - \beta_6}$, $\dot{V}_3 \le 0$. Therefore,

$$V_3 \le \max\left\{V_3(0), \frac{\Xi_\epsilon}{\beta_5 - \beta_6}\right\}, \forall t \ge 0. \tag{47}$$

According to (41), it can be seen that $\frac{1}{2}S^2 \le V_3$. Therefore, $|S| \le \sqrt{\frac{2\Xi_\epsilon}{\beta_5 - \beta_6}}$. It is concluded that closed-loop system is GUUB.

4 Simulation

The MLS dynamic model introduced in Section II was simulated. The simulations were conducted on a personal computer with the setup of Intel Core i7, 3.3 GHz CPU, and 16 GB of RAM. The simulation code was written by Matlab 2016a. Three simulations were performed to evaluate the performance of the control algorithms, including Case I: Sinusoidal trajectory tracking; Case II: Step trajectory tracking; Case III: Sinusoidal disturbance rejection. The uncertainties and its derivations in all cases are bounded. The maximal error (MAE) and the root mean square error (RMSE) are used to evaluate the control accuracy of the system, defined as

$$\text{MAE} = \max_{k=1,2,\cdots,n_k} |r(t_k) - x(t_k)|, \tag{48}$$

$$\text{RMSE} = \sqrt{\frac{1}{n_k}\sum_{k=1}^{n_k} (r(t_k) - x(t_k))^2}. \tag{49}$$

where $r(t_k)$ and $x(t_k)$ are the desired position and the actual position, respectively, and n_k is the number of the sampled data. $t_k = kT_s$ where T_s denotes the sampling interval. T_s is 3×10^{-4} s. All algorithms have same parameters as follows

$$\lambda = 40,\ \Lambda = 150, \kappa = 0.015,$$
$$\Gamma = 8000,\ \Upsilon = 0.1,\ \Gamma_\epsilon = 8000,\ \Upsilon_\epsilon = 0.1. \tag{50}$$

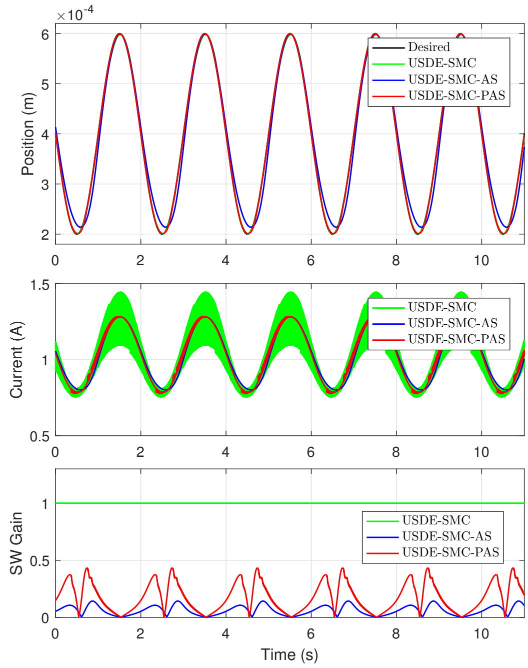

Fig. 3: Simulation results in Case I

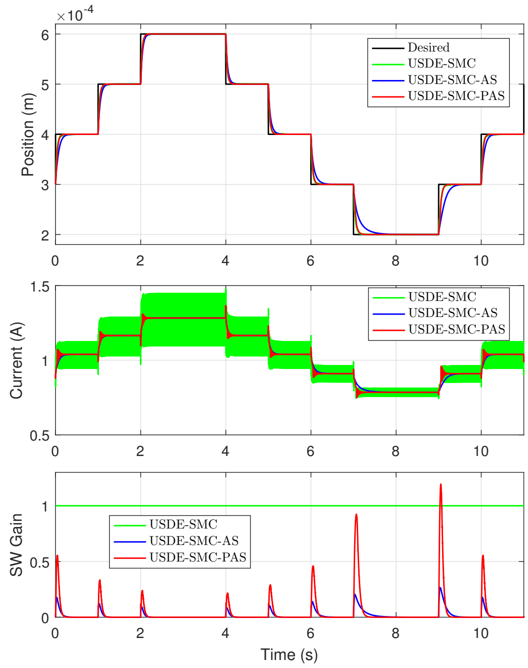

Fig. 4: Simulation results in Case II

In Case I, the MLS is levitated to track a sinusoidal trajectory. The tracking results of Case I are shown in Fig. 3, including tracking position (position), control current (current), and switching gain (SW gain). The numerical results are recorded in Table 2. USDE-SMC-

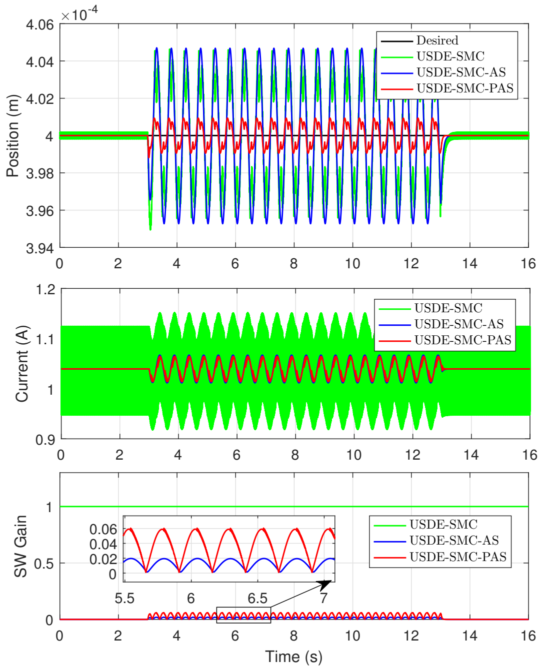

Fig. 5: Simulation results in Case III

Table 2: Numerical results of experiments

		USDE-SMC	USDE-SMC-AS	USDE-SMC-PAS
I	MAE	7.89 μm	35.39 μm	5.36 μm
	RMSE	3.47 μm	18.40 μm	2.15 μm
	Chattering	Obvious	Slight	Slight
II	Max time	0.31 s	0.73 s	0.20 s
	Min time	0.23 s	0.26 s	0.15 s
	Chattering	Obvious	Slight	Slight
III	MAE	5.06 μm	4.73 μm	1.18 μm
	RMSE	2.17 μm	2.61 μm	0.51 μm
	Chattering	Obvious	Slight	Slight

PAS achieves the best tracking accuracy with RMSE and MAE of 5.36 μm and 2.15 μm, respectively, while USDE-SMC-AS has the worst accuracy with RMSE and MAE of 35.39 μm and 18.40 μm, respectively. In Case II, the MLS is levitated to track a step trajectory. The results of Case II are shown in Fig. 4 and Table 2. USDE-SMC-PAS obtains the best dynamic response with the maximum and minimum settling time of 0.20 s and 0.15 s, respectively. In comparison, USDE-SMC-AS has the worst dynamic response with the maximum and minimum settling time of 0.73 s and 0.26 s, respectively. In addition, in Case I and Case II, both USDE-SMC-AS and USDE-SMC-PAS have attenuated chattering phenomenon, while chattering is very obvious in USDE-SMC. The tracking results of Case I and Case II show that PAS can help USDE-SMC-PAS reduce chattering and obtain better tracking accuracy and dynamic response performance than USDE-SMC and USDE-SMC-AS.

In Case III, a sinusoidal disturbance is injected. The results of Case III are shown in Figs. 5 and Table 2. USDE-SMC-PAS has the best disturbance rejection ability. Its RMSE and MAE in Case III are 1.18 μm and 0.15 μm, respectively. In comparison, USDE-SMC and USDE-SMC-AS are relatively worse. In Case III, both USDE-SMC-AS and USDE-SMC-PAS show reduced chattering phenomenon, while USDE-SMC shows very obvious chattering. The disturbance rejection results of Case III show that PAS can help USDE-SMC-PAS obtain stronger disturbance rejection abilities than USDE-SMC and USDE-SMC-AS, with reduced chattering,

5 Experiments and validation

Experiments were conducted on a one-dimensional MLS as shown in Fig. 6. The MLS contains a maglev plant, a Speedgoat (Performance), and two drives (TA115, Trust Automation. Inc.). In the maglev plant, the reluctance actuator used to produce levitation force comprises the bottom E-mover and the I-target, while the reluctance actuator used to generate disturbance force contains the top E-mover and the I-target. The gap x between the bottom E-mover and the I-target is measured by a gap sensor and fed back to Speedgoat. In the MLS, the gap x can change from $7{\times}10^{-4}$ m to $2{\times}10^{-4}$ m, and the main work point is set at the position $r = 4 \times 10^{-4}$ m. The computing time interval T_s is $3{\times}10^{-4}$ s. Three experiments were performed to evaluate the performance of the control algorithms. The uncertainties and its derivations in all cases are bounded. All algorithms have same parameters as follows

$$\lambda = 30,\ \Lambda = 100, \kappa = 0.0137,$$
$$\Gamma = 10000,\ \Upsilon = 0.1,\ \Gamma_\epsilon = 10000,\ \Upsilon_\epsilon = 0.1. \quad (51)$$

To evaluate the ability of USDE-SMC-PAS for dealing with the inherent nonlinearities in an MLS, sinusoidal trajectory tracking experiments and step trajectory tracking experiments were carried out in Case I and Case II, respectively. The motion process and the numerical results of Case I are shown in Fig. 7 and Table 3, respectively. It can be found that the MAE and RMSE of USDE-SMC-PAS are 19.13 μm and 7.70 μm, respectively, and the chattering is slight. When compared to USDE-SMC and USDE-SMC-AS, USDE-SMC-PAS can smoothly track the sinusoidal trajectory with higher accuracy. The tracking results indicate that USDE-SMC-PAS has well-tracking accuracy when

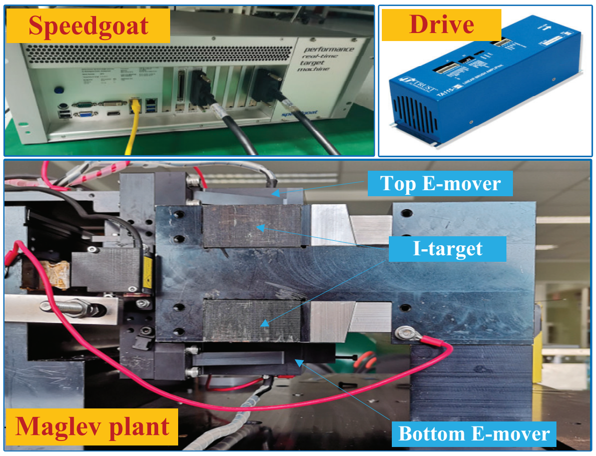

Fig. 6: Experimental setup.

the MLS is guided to a sinusoidal trajectory. The motion process and the numerical results of Case II are shown in Fig. 8 and Table 3, respectively. It can be found that the maximum and minimum settling time of USDE-SMC-PAS are 0.20 s and 0.15 s, respectively, and the chattering is slight. When compared to USDE-SMC, USDE-SMC-PAS has significant advantages in chattering suppression. This benefits from its adaptive switching controller PAS. Compared to USDE-SMC-AS, USDE-SMC-PAS has significant advantages in settling time, which indicates that USDE-SMC-PAS has a better dynamic response by incorporating the filtered estimate error of USDE into the adaptive switching gain.

Table 3: Numerical results of experiments

		USDE-SMC	USDE-SMC-AS	USDE-SMC-PAS
I	MAE	79.04 μm	94.70 μm	19.13 μm
	RMSE	38.03 μm	51.96 μm	7.70 μm
	Chattering	Slight	Slight	Slight
II	Max time	0.41 s	1.61 s	0.32 s
	Min time	0.08 s	0.46 s	0.19 s
	Chattering	Obvious	Slight	Slight
III	MAE	19.87 μm	8.89 μm	1.75 μm
	RMSE	8.46 μm	4.35 μm	0.83 μm
	Chattering	Obvious	Slight	Slight

To evaluate the ability of USDE-SMC-PAS for suppressing the external disturbances in an MLS, disturbance rejection experiments were carried out in Case III, where the sinusoidal disturbance is injected into the MLS by the top reluctance actuator. The disturbance suppression process of Case III are shown in Fig. 9 and Table 3. It can be found that the system with

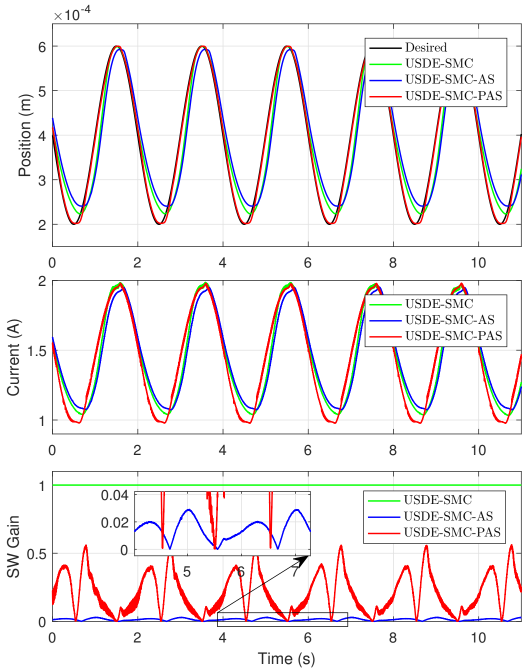

Fig. 7: Experimental results in Case I

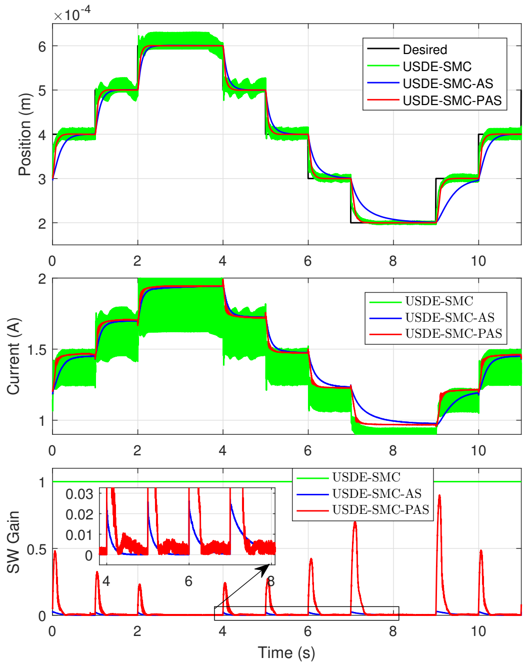

Fig. 8: Experimental results in Case II

USDE-SMC-PAS can smoothly preserve high levitation accuracy with the smallest MAE and the RMSE values when dealing with the disturbance. However, USDE-SMC has obviously chattering phenomena, and its levitation accuracy is bad when the disturbance is injected. USDE-SMC-AS can also reduce chattering, but its improvement of disturbance suppression ability is worse than USDE-SMC-PAS. The results reveal that PAS can help USDE-SMC-PAS reduce the chattering and obtain obvious improvements on the disturbance rejection ability.

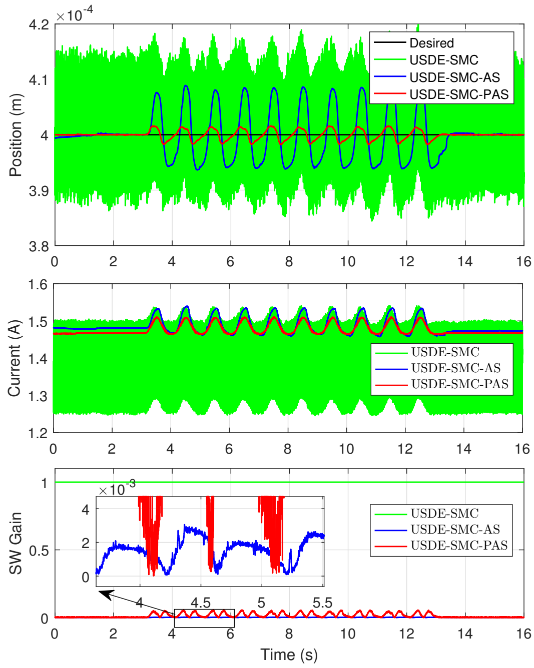

Fig. 9: Experimental results in Case III

The convergence trends of the switching gains ρ in (17), $\hat{K}$ in (23), and $|e_{Lf}| + \hat{\epsilon}$ in (38) are also plotted in the bottom parts of Figs. 7-9. USDE-SMC has a fixed switching gain which is set larger than the upper bound of the uncertainty to obtain sufficient robustness, and thus significant chattering is inevitable. USDE-SMC-AS can adaptively update the switching gain according to the sliding variable, and thus its chattering can be reduced. However, since it is difficult for traditional AS methods to accurately estimate the uncertainty, the disturbances rejection ability of USDE-SMC-AS is not significantly improved. USDE-SMC-PAS embeds the filtered estimate error of USDE into the adaptive switching gain, where the residual part is adaptively updated according to the sliding surface as well. The switching gain of USDE-SMC-PAS can fit the uncertainty more accurately. Therefore, USDE-SMC-PAS has a better dynamic response, higher trajectory tracking accuracy, and stronger disturbance suppression than USDE-SMC and USDE-SMC-AS.

6 Conclusion

This paper proposes a USDE-SMC-PAS to control the MLS with the inherent nonlinearities and external disturbances. The filtered estimate error of USDE and the adaptive part comprise a PAS controller for improving the robustness and dynamic response of MLS. The stabilities of the systems are analyzed by constructing Lyapunov functions. Results of simulations and experiments show that USDE-SMC-PAS can smoothly preserve high levitation accuracy with high dynamic responses when tracking sinusoidal trajectory and step trajectory. In addition, USDE-SMC-PAS behaves better robustness with reduced chattering phenomenon than USDE-SMC and USDE-SMC-AS when dealing with disturbance. With the high control performance and sufficient robustness, the USDE-SMC-PAS method is worth to be recommended to other control applications where inherent nonlinearities and external disturbances are apparent. In addition, the main limitation of the method is that the design of the sliding mode surface is too simple, which may limit the further improvement of the control performance in USDE-SMC-PAS. In the future, we will further optimize the maglev system controller by combining the USDE and PAS with other advanced sliding mode methods, such as terminal SMC, super-twisting SMC, and higher-order SMC and so on.

References

1. X. Chen, W. Ma, S. Luo, Nonlinear Dynamics **101**(4), 2181 (2020)
2. H. Zhou, H. Deng, J. Duan, IEEE/ASME Transactions on Mechatronics **23**(1), 389 (2017)
3. Y. Xu, X. Li, X. Yang, Z. Yang, L. Wu, Q. Chen, Mechanical Systems and Signal Processing **135**, 106427 (2020)
4. F. Beltran-Carbajal, A. Valderrabano-Gonzalez, J. Rosas-Caro, A. Favela-Contreras, ISA transactions **57**, 352 (2015)
5. Z. Junhao, Z. Wen-an, Journal of Systems Science and Mathematical Sciences **37**(8), 1741 (2017)
6. H. Pang, X. Zhang, Z. Xu, ISA transactions **88**, 23 (2019)
7. J. Wang, L. Chen, Q. Xu, IEEE/ASME Transactions on Mechatronics **27**(1), 81 (2022)
8. J. Yang, A. Zolotas, W.H. Chen, K. Michail, S. Li, ISA transactions **50**(3), 389 (2011)
9. Y. Sun, H. Qiang, J. Xu, G. Lin, IEEE Transactions on Industrial Informatics **16**(4), 2629 (2020). DOI 10.1109/TII.2019.2938145
10. P. Roy, B.K. Roy, Journal of Control, Automation and Electrical Systems **31**(3), 597 (2020)
11. X. Liu, H. Yu, Nonlinear dynamics **104**(2), 1429 (2021)
12. F.S. Tabatabaee-Nasab, N. Naserifar, Nonlinear Dynamics **105**(1), 213 (2021)
13. S. Ullah, Q. Khan, A. Mehmood, S.A.M. Kirmani, O. Mechali, ISA transactions **120**, 293 (2022)
14. S. Pandey, V. Dourla, P. Dwivedi, A. Junghare, Nonlinear Dynamics **98**(1), 601 (2019)

15. H. Alipour, M.B.B. Sharifian, H. Afsharirad, Energy and Power Engineering **4**(3), 158 (2012)
16. C. Wang, H. Xia, Y. Wang, S. Ren, Nonlinear Dynamics pp. 1–14 (2021)
17. S. Jain, J.P. Mishra, D. Talange, in *2015 10th Asian Control Conference (ASCC)* (IEEE, 2015), pp. 1–6
18. X. Su, Y. Xu, X. Yang, Mechanical Systems and Signal Processing **168**, 108661 (2022)
19. M.U. Khan, T. Kara, Nonlinear Dynamics **101**(4), 2283 (2020)
20. Y. Sheng, W. Bai, Y. Xie, Nonlinear Dynamics **103**(1), 849 (2021)
21. Y. Huang, J. Na, X. Wu, G. Gao, IEEE Transactions on Industrial Electronics **65**(9), 7258 (2018)
22. F. Ding, J. Huang, Y. Wang, J. Zhang, S. He, Nonlinear Dynamics **90**(4), 2571 (2017)
23. Y. Cao, X. Chen, IEEE/ASME Transactions on mechatronics **19**(3), 924 (2013)
24. J. Chen, Z. Shuai, H. Zhang, W. Zhao, IEEE Transactions on Industrial Electronics **68**(3), 2460 (2021). DOI 10.1109/TIE.2020.2973879
25. K. Shao, J. Zheng, H. Wang, F. Xu, X. Wang, B. Liang, Mechanical Systems and Signal Processing **146**, 107014 (2021)
26. K. Liao, Y. Xu, IEEE Transactions on Industrial Informatics **14**(7), 3076 (2018). DOI 10.1109/TII.2017.2771487
27. Q. Hou, S. Ding, IEEE Transactions on Circuits and Systems II: Express Briefs **68**(2), 747 (2020)
28. J. Na, B. Jing, Y. Huang, G. Gao, C. Zhang, IEEE Transactions on Industrial Electronics **67**(5), 3850 (2019)
29. F. Plestan, Y. Shtessel, V. Bregeault, A. Poznyak, International journal of control **83**(9), 1907 (2010)
30. S. Roy, S.B. Roy, J. Lee, S. Baldi, IEEE/ASME Transactions on Mechatronics **24**(5), 2031 (2019)
31. J. Zhu, K. Khayati, Transactions of the Institute of Measurement and Control **38**(4), 385 (2016)
32. C. Liu, G. Wen, Z. Zhao, R. Sedaghati, IEEE Transactions on Cybernetics **51**(5), 2339 (2020)
33. J. Baek, M. Jin, S. Han, IEEE Transactions on industrial electronics **63**(6), 3628 (2016)
34. S. Roy, S. Baldi, L.M. Fridman, Automatica **111**, 108650 (2020)
35. J. Na, A.S. Chen, G. Herrmann, R. Burke, C. Brace, IEEE Transactions on Vehicular Technology **67**(1), 409 (2017)
36. S. Wang, L. Tao, Q. Chen, J. Na, X. Ren, IEEE/ASME Transactions on Mechatronics **25**(2), 1056 (2020)

7 Statements and Declarations

7.1 Funding

This work was supported in part by National Key R&D Program of China (No.2021YFA1200603), in part by China Postdoctoral Science Foundation (No.2021TQ0070), and in part by State Key Laboratory of ASIC & System, Fudan university (No.2021KF007)

7.2 Competing Interests

The authors have no relevant financial or nonfinancial interests to disclose.

7.3 Data Availability

All data generated or analyzed during this study are included in this published article.